RSC Advances

ROYAL SOCIETY OF CHEMISTRY

www.rsc.org/advances

Novel PVDF hollow fiber ultrafiltration membranes with antibacterial and antifouling properties by embedding N-halamine functionalized multi-walled carbon nanotubes(MWNTs)

Biao Kang[1], Ying-Dong Li[2], Jie Liang[1], Xi Yan[1], Jun Chen[2], Wan-Zhong Lang[1*]

1. The Education Ministry Key Laboratory of Resource Chemistry and Shanghai Key Laboratory of Rare Earth Functional Materials, Department of Chemistry and Chemical Engineering, Shanghai Normal University, 100 Guilin Road, Shanghai 200234, China.
2. College of Life and Environment Sciences, Shanghai Normal University, 100 Guilin Road, Shanghai 200234, China

* Corresponding author. wzlang@shnu.edu.cn (W.Z. Lang); Tel: +86-21-64321951; Fax: +86-21-64321951.

Abstract

Multi-walled carbon nanotubes grafted with (3-chloro-2-hydroxypropyl)-(5,5-dimethylhydantoinyl-1-ylmethyl)-dimethylammonium chloride (MWNTs-g-CDDAC) are doped in PVDF spinning solution to prepare a kind of novel PVDF/MWNTs-g-CDDAC hollow fiber ultrafiltraiton membranes with antibacterial and antifouling properties. The MWNTs-g-CDDAC are firstly synthesized and characterized by FTIR, XPS and TGA. With the addition of MWNTs-g-CDDAC in the dopes, the sponge-like structure is suppressed and the finger-like macrovoids grow wider for the PVDF/MWNTs-g-CDDAC hollow fiber membranes. The surface hydrophlicity and antifouling ability of the membranes are evidently improved by introducing MWNTs-g-CDDAC onto the membranes. The pure water permeability gradually increases with the loading of MWNTs-g-CDDAC in the hybrid membranes, and the highest value of 94.7 $L \cdot m^{-2} \cdot bar^{-1} \cdot h^{-1}$ is obtained with 0.5 wt% MWNTs-g-CDDAC addition in the dope. The permeation flux recovery ratio (R_f) increases with the addition of MWNTs-g-CDDAC, and M-75(0.75wt% MWNTs-g-CDDAC loading in dope) exhibits the highest R_f value of 90.6% after two ultrafiltration-cleaning cycles for BSA aqueous solution. The fabricated PVDF/MWNTs-g-CDDAC membranes have favorable antibacterial efficacy, and M-75 shows the utmost sterilization ratios of 92.7% and 95.2% against E. coli and S. aureus, respectively.

Key words: ultrafiltration; polyvinylidenefluoride(PVDF); multi-walled carbon nanotubes(MWNTs); hollow fiber membrane; antibacterial membrane.

1. Introduction

Over the past years, membrane filtration process has been widely used in water purification and wastewater treatment, and receives considerable attention due to its many superiorities[1]. Nowadays, polyvinylidene fluoride (PVDF) is one intensively used polymer for ultrafiltration membrane preparation owing to its superior anti-oxidation, thermal and hydrolytic stabilities, good mechanical and membrane-forming properties[2, 3]. However, its inherent hydrophobic property often causes severe organic fouling and bio-fouling, which influences the ultrafiltration efficiency, shortens membrane life and restricts the applications of PVDF ultrafiltration membranes. Therefore, it is necessary to improve hydrophilic and antibacterial properties of PVDF membranes. As we all know, biofouling derived from bacteria is a challenge for ultrafiltration processes. To resolve the biofouling problem, several antibacterial species such as silver nanoparticles, titanium dioxide nanoparticles were introduced to modify polymeric membranes[4-10].

Table 1 Some works about polymeric membranes modified with MWNTs and its derivatives published in recent years.

Authors	Polymer	Year	NF/UF/MF	PWFs ($L \cdot m^{-2} \cdot h^{-1}$)	Additive	Antibacterial property
Shawky[11]	PA	2011	NF	32	MWNTs	No
Vatanpour[12]	PES	2011	NF	9 (4 bar)	O-MWNTs	No
Mansourpanah[13]	PES	2011	UF	≈60	PCL-MWNTs	No
Celik[14]	PES	2011	UF	≈160	O-MWNTs	No
Rahimpour[15]	PES	2012	UF	180	F-MWNTs	No
Majeed [16]	PAN	2012	UF	≈67.5	MWNTs	No
Madaeni[17]	PVDF	2013	NF	＜25	MWNTs	No
Gallagher[18]	PVDF	2013	MF	655	MWNTs	No
Vatanpour[19]	PES	2014	NF	≈24.0	NH_2-MWNTs	No
Zhang[20]	PVDF	2014	UF	229.4	O-MWNTs/PFSA	No
Bai[21]	PES	2015	UF	≈340 (60 kPa)	MWNTs-PEG	No
Ghaemi[22]	PES	2015	NF	≈14.0	Polymer wrapped MWNTs	No

In recent years，multi-wall carbon nanotubes(MWNTs) are widely used as nano fillers to modify various polymeric membranes owing to their high surface area, excellent mechanical properties and unprecedented hollow structure. Some works about modified polymeric membranes

using MWNTs and its derivatives as additives are summarized in Table 1. However, the raw MWNTs have poor dispersion performance in the casting solution due to the electrostatic effect. Appropriate chemical modifications can improve its solubility, processibility and allow the unique properties to be coupled with other materials[23].

The oxidation with strong acid is the mostly used method to introduce the oxygen-containing groups and enhance the dispersion and processibility for MWNTs. The blend membranes with oxidized MWNTs usually can improve hydrophilicity, permeability, and mechanical strength[12, 14, 20, 22]. For example, Zhang[20] prepared the PVDF/PFSA/O-MWNTs hollow fiber membranes and studied the synergism of two additives. The hydraulic permeability increases from 100.4 $L \cdot M^{-2} \cdot H^{-1} \cdot bar^{-1}$ to 229.4 $L \cdot M^{-2} \cdot H^{-1} \cdot bar^{-1}$ as O-MWNTs loading increases from 0.25 wt.% to 0.75 wt.% in the dopes. The mechanical strength of the fibers containing O-MWNTs was evidently improved. Celik[14] synthesized MWNTs/polyethersulfone(PES) blend membranes via phase inversion method. They found that the foulant amount on bare PES membranes was 63% higher than the blend membrane with 2% MWCNTs content. Additionally, the oxidized MWNTs can be further grafted with functional groups to endow polymeric membrane with antifouling property[13, 15, 19, 21]. Vatanpour[19] et al. prepared PES nanofiltration membranes embedded by amine-functionalized multi-walled carbon nanotubes(NH_2-MWNTs). The results showed that the hydrophilicity and the pure water flux (PWF) of the nanocomposite membranes were enhanced with the increase of NH_2-MWCNTs addition. Bai[21] and Mansourpanah[13] synthesized PEG-MWNTs and polycaprolactone-MWCNTs(PCL-MWCNTs) respectively. The functionalized MWNTs can evidently improve the performances of PES membranes. From Table 1, the literatures illustrated the recently published works about the polymeric membranes(including MF, UF and NF) modified with MWNTs and its derivatives. However, to our best knowledge, there is little research about grafting MWNTs with organic antibacterial groups and preparing antibacterial membranes. The MWNTs functionalized with organic antibacterial groups would endow the anti-biofouling ability as well as high hydrophilicity and permeability of the resultant composite membranes. In the previous studies, the antibacterial membranes are usually achieved through introducing inorganic metal particles (such as silver and copper nanoparticles) in membrane surfaces or membrane matrix[24-26].

N-halamines, as one kind of antibacterial reagents, receive intensive interests due to its good

biocidal efficacy, regenerability, non-toxicity to humans and relatively low expense[27]. They were usually grafted on polymers (such as cellulose, polyurethane, nylon 6, aromatic polyamide) to prepare antibacterial materials[28-31]. For example, the quaternarized N-halamine precursor (3-chloro-2-hydroxypropyl)-(5, 5-dimethylhydantoinyl-1-ylmethyl)-dimethylammonium chloride (CDDAC) was grafted onto cellulose to prepare antimicrobial fabric [28].

In this work, MWNTs were oxidized by Fenton reagent (H_2O_2/Fe^{2+}) to introduce abundant hydroxyl groups on their surfaces according the previous literature [32]. Then, the self-synthesized CDDAC was grafted on the oxidized MWNTs to improve their solubility and processibility, and endowed them with antibacterial property. The MWNTs grafted with CDDAC (MWNTs-g-CDDAC) were employed to modify PVDF and prepared PVDF/MWNTs-g-CDDAC hollow fiber ultrafiltration membranes with antibacterial and antifouling properties. The effects of MWNTs-g-CDDAC addition on the morphology, surface hydrophilicity, permeation and antifouling performance of the resultant membranes were investigated. The antibacterial efficacy of membranes was evaluated against Gram-negative E. coli and Gram-positive S. aureus.

2. Materials and methods

2.1. Materials

PVDF in powder was purchased from Shanghai 3F New Material Co. Ltd. (China). MWNTs (L-MWNT-2040, purity>97%) with the diameter of 20–40 nm and the average length of 5–15 μm were obtained from Shenzhen Nanotech Port Co. Ltd. (China). 1-(hydroxymethyl)-5,5-dimethylhydation was purchased from Tokyo Chem. Ind. Co., Ltd. Five polyethylene glycols (PEGs) (M_w=2 kDa, 6 kDa, 10 kDa, 20 kDa and 35 kDa) and one polyethylene oxide (PEO, M_w=100 kDa) were purchased from Sigma-Aldrich Trading Co. Ltd. Bovine serum albumin (BSA, M_w=67 000) was purchased from Shanghai Bio Co. Ltd. (China). Other chemicals were purchased from Shanghai Chemical Agent Company (China).

2.2. Synthesis and characterizations of MWNTs-g-CDDAC

The original MWNTs were purified with 0.5 M HCl aqueous solution. Then, the purified MWNTs were oxidized with Fenton reagent (mass ratio, H_2O_2/Fe^{2+}=1:1) at 25 ^oC for 8 h to introduce hydroxyl groups (-OH) (recorded as MWNTs-OH). The MWNTs-OH were filtered, rinsed and dried at 40 ^oC for 24 h.

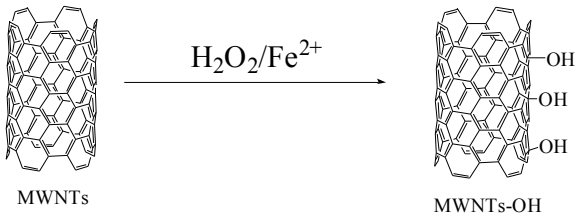

Fig. 1 The schematic diagram of MWNTs-OH.

The synthesis of CDDAC was carried out according to the proposed procedure by Kang *et al*.[33]. In a typical synthesis process of CDDAC, 0.10 mol 1-hydroxymethyl-5,5-dimethylhydantoin reacted with 0.12 mol dimethylamine at 25°C for 4h with isopropanol as solvent. After removing isopropanol and unreacted dimethylamine with the aid of reduced pressure distillation, (5,5-dimethylhydantoinyl-1-ylmethyl)-dimethylamine (DHDA) was obtained. Then, the obtained DHDA was reacted with 0.10 mol epichlorohydrin. The reaction products were purified to obtain CDDAC. Generally, the yield of CDDAC could be achieved above 85%, which can be obtained by silver nitrate titration method[33].

10.0g CDDAC and MWNTs-OH were dissolved in 500 mL deionized water and sonicated for 0.5 h. Then, the mixture was collected and dried at 100 °C for 10 h, and further treated at 200 °C for 2 h to obtain MNWTs-g-CDDAC. After the above mentioned procedures, the MWNTs-g-CDDAC were soaked in 0.5 wt.% detergent solution for 15 min, then washed with deionized water repeatedly to remove free CDDAC and detergent. Finally, they were vacuum-dried at 90 °C overnight. The synthesis procedure of MNWTs-g-CDDAC can be illustrated in Fig.2.

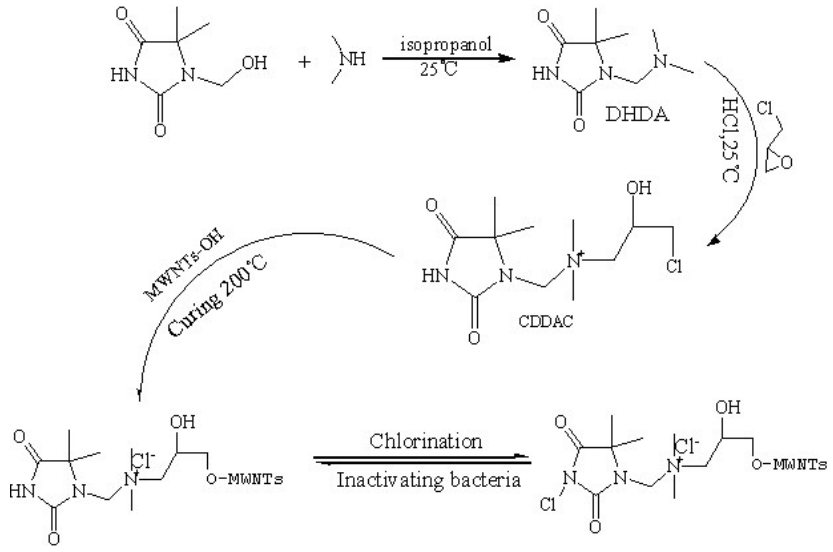

Fig. 2 The synthesis route of MWNTs-g-CDDAC.

2.3. Preparation of PVDF/MWNTs-g-CDDAC hollow fiber membranes

The dope solutions were prepared with 18.0 wt% PVDF and different amounts of MWNTs-g-CDDAC (0.0 wt%, 0.25 wt%, 0.50 wt.% and 0.75 wt.%). The residual was balanced with NMP solvent. The mixtures were intensively stirred at 70 ^{o}C for 12 h to obtain homogeneous dopes.

The hollow fiber membranes were fabricated at 25 ^{o}C by wet spinning process. The dope compositions and the spinning conditions of PVDF/MWNTs-g-CDDAC hollow fiber membranes were presented in Table 2 and Table 3, respectively. All the newly spun fibers were stored in deionized water for 24h to remove the residual solvent. After that, the membranes were doped in 50 wt.% glycerol aqueous solution for 24 h to avoid the structure collapse.

Table 2 The doping compositions of PVDF/MWNTs-g-CDDAC hollow fiber membranes.

Membrane no.	Doping compositions (PVDF/MWNTs-g-CDDAC/NMP)	Bore fluid (NMP/H_2O)
M-00	18.00/0.00/82.00	90/10
M-25	18.00/0.25/81.75	90/10
M-50	18.00/0.50/81.50	90/10
M-75	18.00/0.75/81.25	90/10

Table 3 Spinning parameters of PVDF/MWNTs-g-CDDAC hollow fiber membranes.

Parameters	Values
Nitrogen pressure (MPa)	0.3
Bore fluid flow rate (mL/min)	0.6
Bore fluid temperature (^{o}C)	25
Air gap (cm)	0
Coagulation bath	Tap water
Coagulation bath temperature(^{o}C)	25

2.4. Characterizations of MWNTs-g-CDDAC

The MWNTs, MWNTs-OH and MWNTs-g-CDDAC were detected by a Fourier Transform Infrared Spectroscopy (FTIR, ElectronCorp Nicolet 380) in the wavenumber of 500–3700 cm^{-1} and X-ray photoelectron spectroscopy (XPS, Perkin-Elmer PHI 5000C ESCA) using Al Kα radiation. The C_{1s} spectrum at 284.8 eV as an internal standard was employed in XPS characterizations.

Thermal gravimetric analysis (TGA, DSCQ100 TA Instruments) was conducted in N_2 atmosphere to evaluate the thermal stability of MWNTs, MWNTs-OH and MWNTs-g-CDDAC. The samples were heated from 35 to 800 ^oC with the heating rate of 10 ^oC/min.

2.5. Characterizations of PVDF/MWNTs-g-CDDAC hollow fiber ultrafiltration membranes

2.5.1. Morphologies of PVDF/MWNTs-g-CDDAC hollow fiber ultrafiltration membranes

The rheology properties of the dopes were tested by a rotational rheometer (Austria Anton Paar MCR102) at room temperature. The morphologies of PVDF/MWNTs-g-CDDAC hollow fiber ultrafiltration membranes were observed by a field emission scanning electronmicroscopy (FESEM, Hitachi S-4800). The fibers were soaked in deionized water for 30 min to remove glycerol and other solvents. Then the fibers were immersed in ethanol for 10 min and quickly fractured to obtain a clear cross-section. The samples were placed on a metal holder and gold-coated under vacuum before testing.

2.5.2. Dynamic contact angle

The hydrophilicity of PVDF/MWNTs-g-CDDAC hollow fiber membranes was measured on the outer surfaces by sessile drop method, which was performed on a contact angle analyzer (KRUSS DSA30 German). The contact angle experiments were conducted via a droplet of 2.0 μL at room temperature. All the results were recorded in movies for 600 s and repeated for three times.

2.5.3. Permeation performances of PVDF/MWNTs-g-CDDAC hollow fiber ultrafiltration membranes

The permeation experiments were conducted over homemade ultrafiltration system, which was presented in previous works[20, 34, 35]. All the experiments were performed at 25±1 ^oC with a feed pressure of 1.0 bar. The newly fabricated fibers were pre-pressured at 2.0 bar with deionized water for 30 min before testing. The pure water permeability (J_w) and rejection (R) were defined as formulas (1) and (2), respectively

$$J_w = \frac{Q}{\Delta P \times A \times t} \quad (1)$$

$$R = 1 - \frac{C_P}{C_F} \quad (2)$$

where Q and ΔP are the volumetric flow rate ($L \cdot m^{-2} \cdot bar^{-1} \cdot h^{-1}$) and the transmembrane pressure (bar), respectively, A is the valid membrane area (m^2), R represents the rejection of solute, and C_P and C_F represent the concentrations of permeate and feed solutions, respectively.

2.5.4. Pore size, pore size distribution, molecular weight cut-off (MWCO) and porosity of PVDF/MWNTs-g-CDDAC hollow fiber membranes

Commonly, the permeation performances of membranes were mainly determined by their pore sizes [36]. The solute rejection experiments were performed to detect the pore size, pore size distribution and molecular weight cut-off (MWCO) of PVDF/MWNTs-g-CDDAC membranes. In this test, five PEGs(Mw: 2 kDa, 6 kDa, 10 kDa, 20 kDa and 35 kDa) and one PEO (Mw: 100 kDa) were used as solutes. A TOC analyzer (Shimadzu TOC-V CPN, Japan) was used to measure the concentrations of permeate and feed solutions. The details were mentioned in the previous articles[20, 37]. The membrane porosity ε **(%)** was defined using gravimetric method [38].

2.5.5. Antifouling measurement

The cyclic ultrafiltration-regeneration tests were performed to evaluate the antifouling ability of PVDF/MWNTs-g-CDDAC membranes. First, the membranes were fouled by the filtration process with 500 ppm BSA aqueous solution for 30 min. Then the fouled membranes were washed with 50 ppm NaOCl solution using cleaning in place procedure (CIP) at room temperature. The pure water fluxes of the membranes were measured again after washing for 30 min. The pure water flux recovery ratio (R_f) was obtained to study the recovery ability of membrane after BSA fouling. It can be calculated by the ratio of the final water flux versus the initial one.

2.5.6. Assessments of oxidative chlorine and antibacterial efficacy

The contents of oxidative chlorine (Cl^+) of membrane samples were determined by a standard iodometric/thiosulfate titration procedure[39]. A small membrane sample (cut into pieces, about 1.0 g) was suspended in 150 mL sulfuric acid solution (0.04 $mol \cdot L^{-1}$). After adding 0.50 g potassium iodide and 0.40 mL starch solution (0.50 wt.%) as an indicator, the solution was titrated with sodium hyposulfite solution (0.01 $mol \cdot L^{-1}$) until the blue color disappeared at the end point. The

Cl^+ content of the sample could be calculated using the following equation:

$$Cl^+ = \frac{35.45 \times N \times V}{2 \times W} \times 100\% \quad (3)$$

where N and V stand for the normality (eqv/L) and volume (L) of the consumed $Na_2S_2O_3$ in the titration, and W is the weight of membrane sample.

The antibacterial ability of the fibers was evaluated by the shake flask method[40]. This method assesses the variation of bacteria concentration by measuring the optical density (OD) of nutrient broth at 600 nm after placing the sample in a shaking flask for 24 h. A typical procedure was conducted in the following way. 0.10 g fiber sample, cut into small pieces with a length of approximately 1.0 mm, was immersed into a flask containing 50 mL beef extract peptone. Then the flasks were sterilized in an autoclave. Afterwards, 100μL bacterial suspension (10^6 CFU/mL) was added into the flask. Then the flasks were shaken at 200 rpm on a rotary shaker at 37 ^oC for 24 h. After incubation, the absorbance of bacteria concentration was measured with an UV spectrophotometer at 600 nm. The bacteriostasis ratio was calculated via the following equation:

$$E = \left(1 - \frac{n_1}{n_0}\right) \times 100\% \quad (4)$$

where E represents the percentage of bacterial reduction, n_0 is the absorbance values of live bacterial cells in the flask contained the bare membrane(M-00), n_1 is the absorbance value of live bacterial cells in the flask contained various hybrid membranes (M-25~M-75).

In order to visually display the antibacterial efficiency, the flat membranes with the same compositions as those of M-00, M-25, M-50 and M-75 were cast and called as FM-00, FM-25, FM-50 and FM-75 respectively. The antibacterial ability of the cast flat membranes was carried out as follows. 50μL E. coli suspension (10^6 CFU/mL) was inoculated on the agar plate by spread plate method. The diameter of 10.0 cm round flat membrane was placed on agar plate. The colonies on plates were counted after incubation at 37 ^oC for 24 h. The bacteriostasis ratio (E) was also calculated by equation (4), where n_0 and n_1 are the numbers of colonies on the petri dishes with flat pristine PVDF membrane and PVDF/MWNTs-g-CDDAC membranes, respectively.

3. Results and discussions

3.1. Characterizations of MWNTs-g-CDDAC

Fig. 3(a) illustrates the FTIR spectra of MWNTs, MWNTs-OH and MWNTs-g-CDDAC. As shown in Fig.3(a), the two absorption peaks at 3420 and 1637 cm^{-1} in the spectrum of MWNTs are attributed to the stretch vibration of hydroxyl and C=C respectively. The peak at 1401 cm^{-1} for MWNTs-OH is associated with the bending deformation of -OH groups[41], which are introduced by the Fenton oxidation process. For the spectrum of MWNTs-g-CDDAC, the bands at 1718 cm^{-1} and 1766 cm^{-1} should be attributed to the carbonyl groups of the amide structure on the hydantoin ring[42-44]. The peak at 1391 cm^{-1} corresponds to the vibration of methyl groups.

As displayed in Fig.3(b), MWNTs-OH and MWNTs-g-CDDAC are both well dispersed in absolute NMP. MWNTs-OH is easily dispersed in NMP because of the strong hydrogen bonds between NMP and MWNTs-OH, and oxygen-containing functional groups (carboxyl and hydroxyl groups) prevent the direct aggregation among MWNTs-OH[20]. As for MWNTs-g-CDDAC, the dispersion is further enhanced due to the presence of halamine groups in MWNTs-g-CDDAC[45].

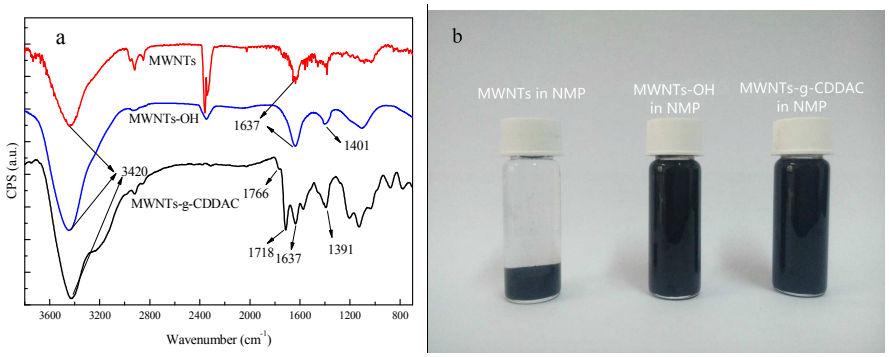

Fig. 3 The FTIR spectra of MWNTs, MWNTs-OH and MWNTs-g-CDDAC (a); the digital photos of MWNTs, MWNTs-OH and MWNTs-g-CDDAC dispersed in absolute NMP for 30 days (b).

The overall and narrow XPS spectra of MWNTs, MWNTs-OH and MWNTs-g-CDDAC are shown in Figs.4-5 respectively. In the overall XPS spectra, the intensive C1s peaks are observed for all three samples. Apart from the intensive C1s peaks, additional peaks at 531.9 eV attributed to O1s are observed in the XPS spectra of MWNTs-OH and MWNTs-g-CDDAC, implying that the oxygen-containing groups are successfully introduced on MWNTs by Feton method. From the narrow spectra of the samples in Fig.5, the peaks at 198.9 eV and 399.7 eV are observed and ascribed to Cl2p3/2 and N1s for MWNTs-g-CDDAC[46], implying that CDDAC is introduced to the surfaces of MWNTs-OH by the chemical reaction in Fig.2.

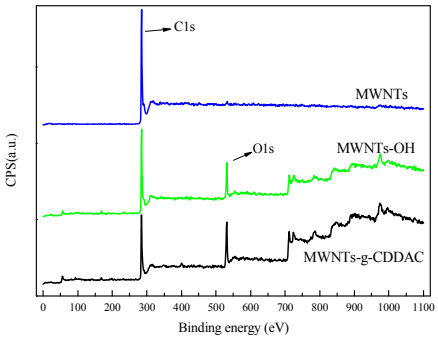

Fig. 4 The overall spectra of purified MWNTs, MWNTs-OH and MWNTs-g-CDDAC.

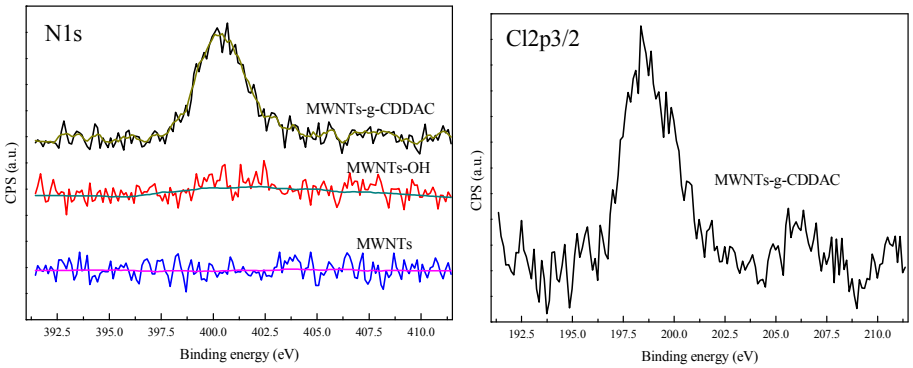

Fig. 5 The single element spectra of MWNTs, MWNTs-OH and MWNTs-g-CDDAC.

The TGA curves of MWNTs, MWNTs-OH and MWNTs-g-CDDAC are shown in Fig. 6. MWNTs exhibits the highest thermal stability and a single weight loss above ~620 ^{o}C. The weight loss of MWNTs-OH can be divided into two stages. The first stage below 250 ^{o}C can be ascribed to the evaporation of free water and adsorbed water in MWNTs-OH. The second stage over 450 ^{o}C should be attributed to the decomposition of MWNTs-OH. The thermal weight loss of MWNTs-g-CDDAC can be roughly divided into three stages: below 250 ^{o}C, 300~450 ^{o}C and over 530 ^{o}C. The similar downward trend in MWNTs-OH at the first stage owing to the evaporation of free water and adsorbed water is also found in MWNTs-g-CDDAC. At the second stage, there is an obvious down-trend with the increase of temperature, which is primarily attributed to the decomposition of hydantoin groups. After increasing over 530 ^{o}C, the TGA curve performs a dramatic decline due to the thermolysis of carbon nanotubes. In contrast to MWNTs and MWNTs-OH, the TGA of MWNTs-g-CDDAC displays obviously downward trend, implyinging that new groups were introduced on the surfaces of MWNTs.

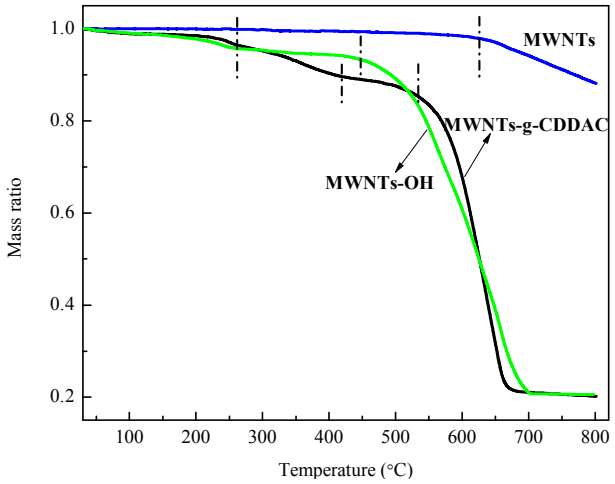

Fig. 6 The TGA curves of MWNTs, MWNTs-OH, MWNTs-g-CDDAC.

3.2 Characterizations of PVDF/MWNTs-g-CDDAC hollow fiber membranes

3.2.1 Morphologies of PVDF/MWNTs-g-CDDAC hollow fiber membranes

Commonly, the phase separation process is closely related to the rheology property of dope solution. Fig. 7 shows the effect of MWNTs-g-CDDAC loading in the dopes on the viscosity versus shear rate. It can be seen that the apparent viscosity of the dopes decreases with the increase of shear rate due to shear-thinning mechanism[20, 47]. Also, the apparent viscosity gradually increases as the MWNTs-g-CDDAC loading increases, implying that MWNTs-g-CDDAC has good affinity with PVDF chains in dopes[20, 48]. It can be explained that the added MWNTs-g-CDDAC restrain the shear flow of PVDF chains and result in the increase of shear viscosity[49].

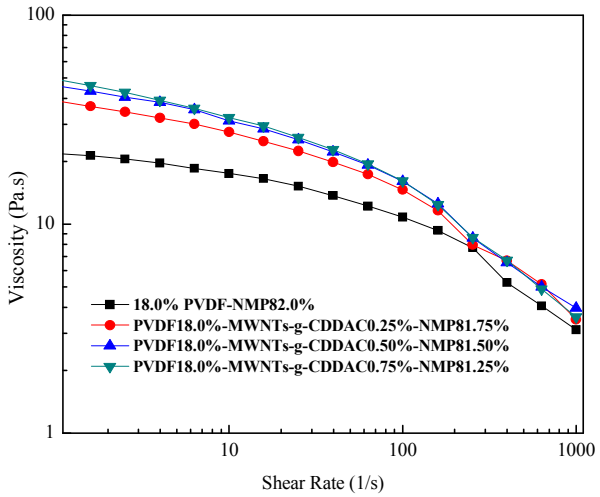

Fig. 7 The viscosity versus shear rate of different dope solutions.

The FESEM images of the cross-sections, outer and inner surfaces of PVDF/MWNTs-g-CDDAC hollow fiber membranes are displayed in Figs.8-10 respectively. Due to the strong nonsolvent effect of water (outer coagulation liquid), the phase separation process immediately begins from the outer side when the dopes are extruded into water bath. However, 90.0% NMP aqueous solution as bore liquid almost cannot lead to the demixing of the dopes. The demixing behavior leads to the finger-like voids go through the whole cross-sections and the resultant asymmetrical structure. From Fig. 8, the cross-sections of fibers can be roughly divided into three-layer structure: skin layer, sub-layer layer and macrovoid layer, which are indicated in the FESEM image of M-25. Compared with other three fibers, the fiber of M-00 without MWNTs-g-CDDAC has much sponge-like structure in the cross-section near the inner side. With the addition of MWNTs-g-CDDAC, the sponge-like structure almost disappears and the cross-section exhibits the typical three-layer structure for M-25. As the MWNTs-g-CDDAC addition further increases, the finger-like macrovoids grow wider and the number increases. It can be explained that the increased dope viscosity restricts the outdiffusion of solvent with MWNTs-g-CDDAC addition and causes a wider structure of finger-like macrovoids[14, 20].

The FESEM images of the outer and inner surfaces of PVDF/MWNTs-g-CDDAC hollow fiber membranes are illustrated in Figs. 9-10. Owing to the strong polarity of water (outer coagulation liquid), the dense outer surfaces are formed for all the fibers, which will act as the separation skin layer. However, the porous reticulation structures are found on the inner surfaces because no demixing of the dopes occurs from inner side using 90 wt.% NMP aqueous solution as bore liquid[20]. These porous inner surfaces provide the foundation to obtain high permeation flux for the PVDF/MWNTs-g-CDDAC hollow fiber ultrafiltration membranes.

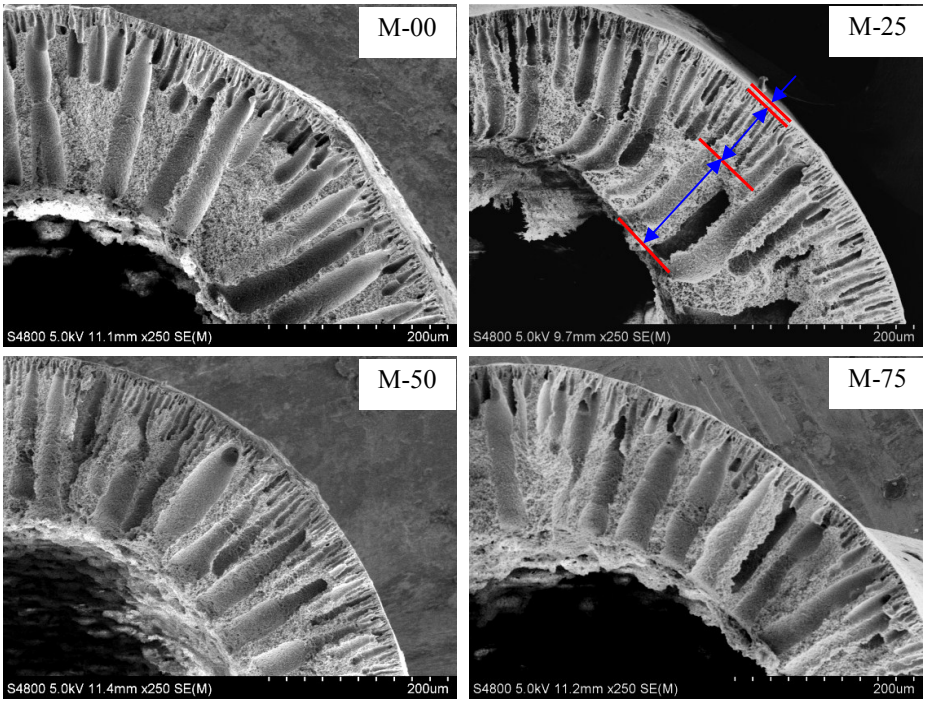

Fig. 8 The FESEM images of the cross-section of PVDF/MWNTs-g-CDDAC hollow fiber membranes.

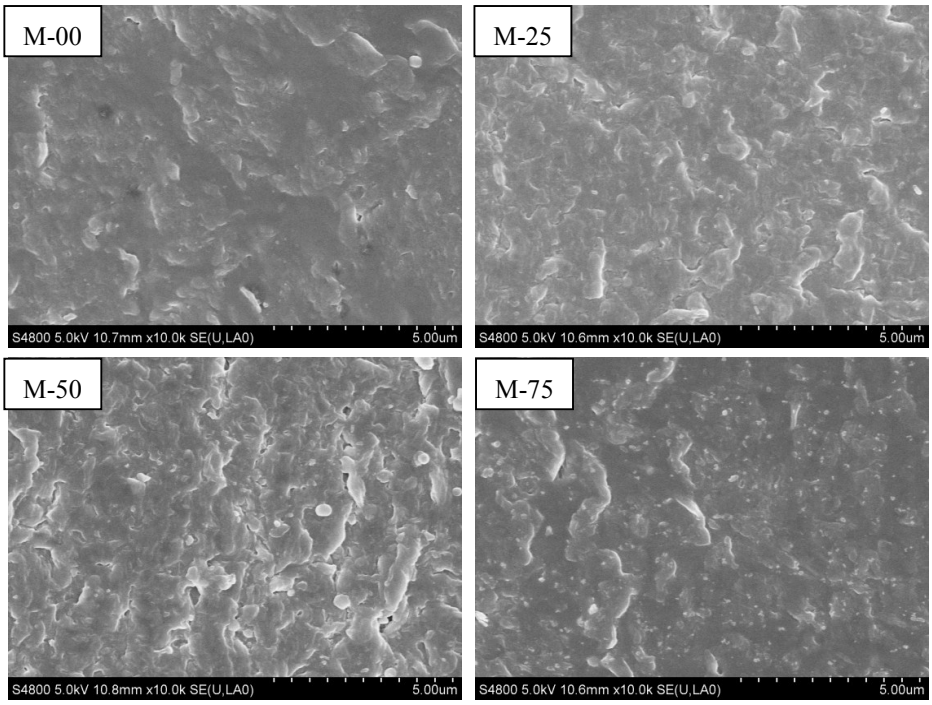

Fig. 9 The FESEM images of the outer surfaces of PVDF/MWNTs-g-CDDAC hollow fiber membranes.

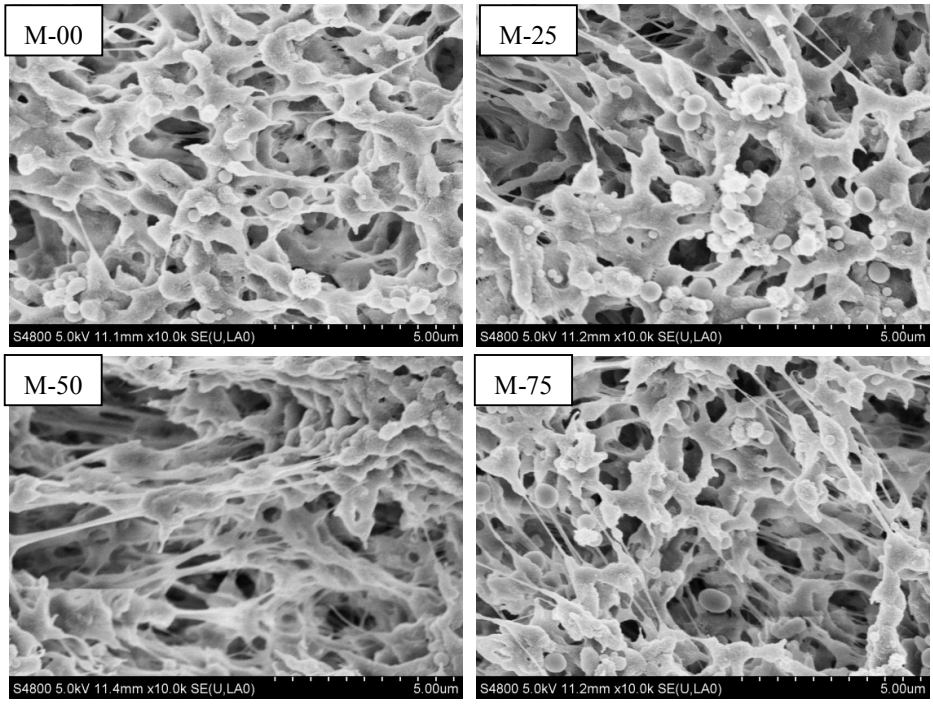

Fig. 10 The FESEM images of the inner surfaces of PVDF/MWNTs-g-CDDAC hollow fiber membranes.

3.2.2. Dynamic contact angle

As we all know, the hydrophilicity markedly influences the permeability and antifouling ability of polymeric membranes[50, 51]. The dynamic contact angles of the outer surfaces of fibers are shown in Fig. 11. The membrane of M-00 exhibits the highest contact angle with a final value of 75.8°, indicating that pristine PVDF membrane without MWNTs-g-CDDAC presents more hydrophobic surface. With the addition of MWNTs-g-CDDAC in dopes, the surface contact angle evidently decreases, implying the increase of surface hydrophilicity of PVDF/MWNTs-g-CDDAC hybrid membranes. The increased hydrophilicity should be attributed to affinity between the hydrophilic moieties (such as -R_2NH) of MWNTs-g-CDDAC and water molecules. The final contact angles of M-25, M-50 and M-75 attain 57.6°, 50.9° and 38.2° respectively. The improved surface hydrophilicity will promote the infiltration and permeability of PVDF/MWNTs-g-CDDAC membranes.

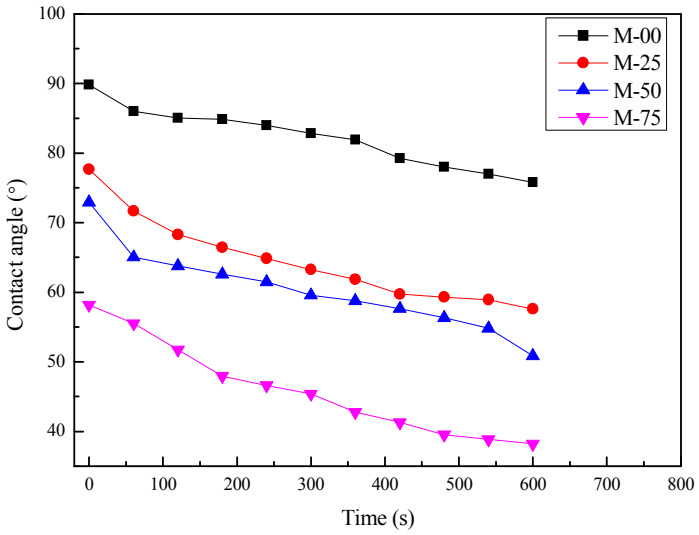

Fig. 11 The dynamic contact angles of PVDF/MWNTs-g-CDDAC hollow fiber membranes.

3.2.3. Pore size, pore size distribution and molecular weight cut-off (MWCO) of PVDF/MWNTs-g-CDDAC hollow fiber membranes

The pure water permeability (J_w), pore size (d_p) and molecular weight cut-off (MWCO) of the prepared PVDF/MWNTs-g-CDDAC hollow fiber membranes are shown in Fig. 12. The results demonstrate that the pristine PVDF membrane (M-00) has a J_w of 44.9 $L \cdot m^{-2} \cdot bar^{-1} \cdot h^{-1}$. With the addition of MWNTs-g-CDDAC, the J_w gradually increases to 53.2 $L \cdot m^{-2} \cdot bar^{-1} \cdot h^{-1}$ for M-25, 94.7 $L \cdot m^{-2} \cdot bar^{-1} \cdot h^{-1}$ for M-50 and then dramaticly decreases to 54.6 $L \cdot m^{-2} \cdot bar^{-1} \cdot h^{-1}$ for M-75. In general, the hydraulic permeability is related to the structure, pore size, and the surface hydrophilicity of membranes. M-00 exhibits less finger-like voids in the cross-section and the lowest hydrophilicity compared to other membranes, which leads to the lowest J_w value for M-00.

From Table 4, the d_p value decreases from 10.8 nm to 8.9 nm as the addition of MWNTs-g-CDDAC increases from 0.0wt.% to 0.50wt.% for M-00 and M-50, and then slightly increases to 9.1 nm with 0.75wt.% addition of MWNTs-g-CDDAC. The same trend of MWCO values is also found for the PVDF/MWNTs-g-CDDAC hollow fiber membranes. The porosity of PVDF/MWNTs-g-CDDAC hollow fiber membranes varies little and attains about 80%. Associating the variation of J_w with d_p values, it can be concluded that the hydraulic permeability of membrane is determined by the pore size as well as the participation of MWNTs-g-CDDAC.

Furthermore, with the increase of MWNTs-g-CDDAC loading, the highest hydraulic permeability is obtained for M-50. The σ values reflect the pore size distribution error, which means the uniformity degree of membrane pores. It can be insinuated that the dispersion of MWNTs-g-CDDAC would affect pore forming, which provides more pores per area of membrane surface[20, 34].

Table 4 The pure water permeability, porosity, pore size, geometric standard deviation and molecular weight cut-off (MWCO) of PVDF/MWNTs-g-CDDAC hollow fiber membranes.

Membrane no.	J_w (L·m^{-2}·bar^{-1}·h^{-1})	d_p(nm)	σ	MWCO(kDa)	ε (%)
M-00	44.9 ± 3.1	10.8	1.53	84.9	79.32±0.54
M-25	53.2 ± 4.2	9.7	1.61	79.0	80.02±0.82
M-50	94.7 ± 5.6	8.9	1.72	78.4	80.71±1.50
M-75	54.6 ± 4.7	9.1	1.76	86.6	80.39±0.96

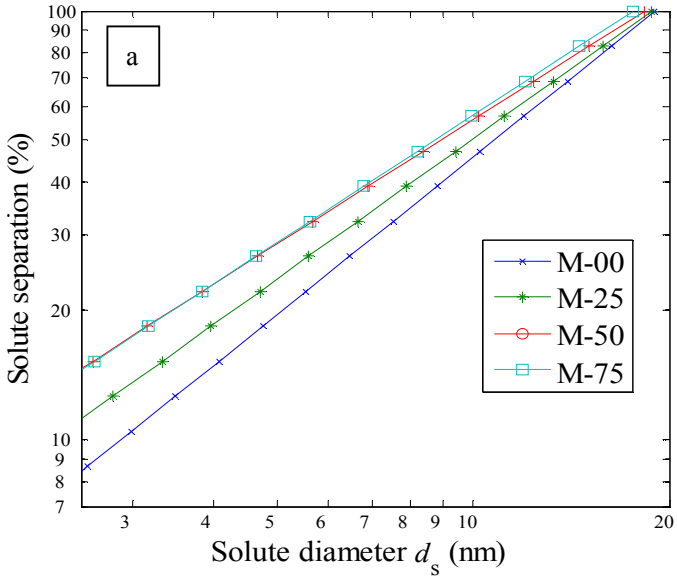

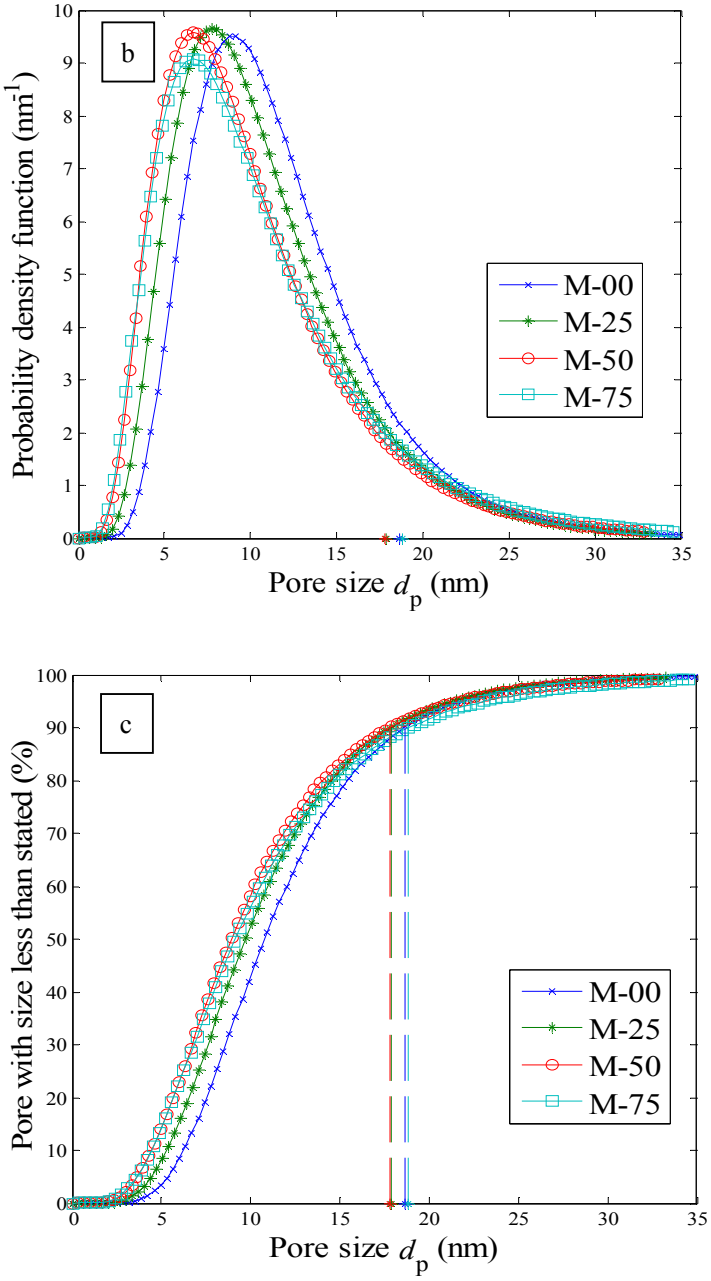

Fig. 12 Solute PEG rejection curves (a), probability density function curves (b) and cumulative pore size distribution curves (c) of PVDF/MWNTs-g-CDDAC hollow fiber membranes.

3.2.4 Flux decay and regeneration of PVDF/MWNTs-g-CDDAC hollow fiber membranes

The antifouling results of PVDF/MWNTs-g-CDDAC hollow fiber membranes are displayed in Fig. 13 and Table 5. During the process of filtraiton, the permeation fluxes of all the membranes for BSA aqueous solution decrease sharply owing to concentration polarization and membrane fouling[20]. From Table 5, compared with the pristine membrane (M-00), the membranes of M-25,

M-50 and M-75 have much higher R_f values than that of M-00. Additionally, the R_f value also slightly increases with the addition of MWNTs-g-CDDAC, and M-75 exhibits the highest R_f value of 90.6% after whole fouling and cleaning experiment. These results verify that using MWNTs-g-CDDAC to modify PVDF membranes can evidently improve the antifouling property of the obtained PVDF/MWNTs-g-CDDAC hollow fiber membranes. From Table 5, it also can be seen that all the PVDF/MWNTs-g-CDDAC hollow fiber membranes exhibit very high BSA rejection, implying that good ultrafiltration performance can be got.

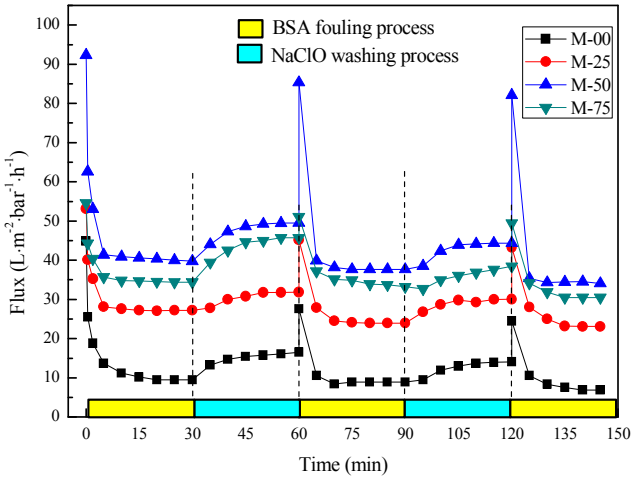

Fig. 13 Time-dependent flux of PVDF/MWNTs-g-CDDAC hollow fiber membranes with ultrafiltration and cleaning cycles.

Table 5 The antifouling testing details of PVDF/MWNTs-g-CDDAC hollow fiber membranes.

Membrane no.	1st BSA rejection (%)	1st R_f (%)	2nd BSA rejection (%)	2nd R_f (%)	3rd BSA rejection (%)
M-00	93.4±3.9	61.4±4.7	96.7±4.5	54.6±3.3	97.6±4.0
M-25	94.9±4.4	84.9±3.2	96.1±4.9	81.4±3.8	97.0±3.4
M-50	97.1±3.1	90.1±4.4	98.1±3.2	86.7±3.6	98.3±4.5
M-75	97.8±2.5	93.6±5.3	98.6±4.6	90.6±4.5	99.3±3.7

3.2.5. Assessment of oxidative chlorine and antibacterial efficacy

Table 6 The Cl^+ contents and sterilization ratios of PVDF/MWNTs-g-CDDAC hollow fiber ultrafiltration membranes (shake flask method).

Membrane no.	Cl^+ content (mmol/g)	Sterilization ratio(E)	
		Against E. coli (%)	Against S. aureus (%)
M-00	0.00	-10.6 ± 3.2	-9.97 ± 2.5
M-25	0.17±0.02	74.1 ± 6.7	75.8 ± 3.4
M-50	0.29±0.05	88.3 ± 4.5	89.6 ± 5.1
M-75	0.43±0.04	92.7 ± 3.9	95.2 ± 2.2

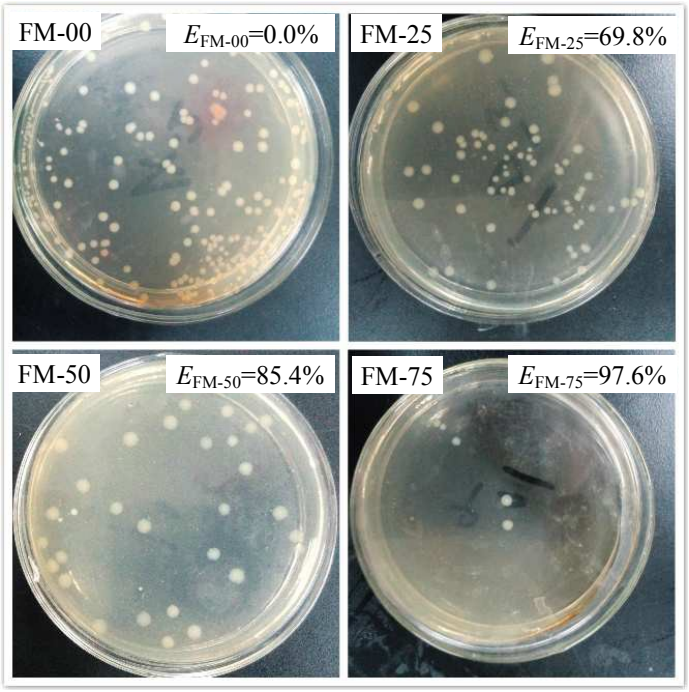

Fig. 14 The antibacterial efficiency against E. coli of PVDF/MWNTs-g-CDDAC flat membranes (spread plate method).

Table 7 The stability testing of M-75.

Standing time(days)	Cl^+ content (mmol/g)
0	0.43±0.04
3	0.41±0.04
6	0.39±0.06
9	0.37±0.04

The antibacterial ability of MWNTs-g-CDDAC is accomplished by the direct transfer of positive chlorines (Cl^+) from N-halamines to the appropriate receptors in cells[27, 52]. The contents of

Cl^+ in PVDF/MWNTs-g-CDDAC hollow fiber membranes and antibacterial efficiency are shown in Table 6. The sterilization ratios of PVDF/MWNTs-g-CDDAC hollow fiber membranes are determined by the shake flask method. From Table 6, the Cl^+ contents of the PVDF/MWNTs-g-CDDAC hollow fiber ultrafiltration membranes almost linearly increases with the addition of MWNTs-g-CDDAC in the samples, which guarantee the antibacterial efficiency of the hybrid membranes. The stability testing of M-75 with respect to standing time is shown in Table 6. After 9 days storage in the air, the Cl^+ content of M-75 slightly decreases from the initial value of 0.43 $mmol \cdot g^{-1}$ to final one of 0.37 $mmol \cdot g^{-1}$, which is still high enough to quickly kill bacteria.

Since PVDF has no antibacterial ability, it may provide sites for cells to breed. Therefore, M-00 exhibits no sterilization efficiency against E. coli and S. aureus. The results in Table 6 indicate that the sterilization ratios against both E. coli and S. aureus increase with the addition of MWNTs-g-CDDAC. M-75 shows the utmost sterilization ratios of 92.7% and 95.2% against E. coli and S. aureus respectively, which indicates that the PVDF/MWNTs-g-CDDAC hybrid membranes have antibacterial properties against both Gram-positive bacteria and Gram-negative bacteria.

The antibacterial efficacy of the flat membranes of FM-00, FM-25, FM-50 and FM-75 against E. coli is visually shown in Fig.14, which is conducted by the spread plate method[53]. From Fig. 14, the membrane FM-00 is covered with much more bacterial colonies, indicating that the pristine PVDF membrane without MWNTs-g-CDDAC has no inhibition effect against the growth of E. coli. With the addition of MWNTs-g-CDDAC in the hybrid membranes, compared with FM-00, the colonies of E. coli on the surfaces of FM-25, FM-50 and FM-75 dramatic decline, and the sterilization ratio attains 69.8%, 85.4% and 97.6% respectively.

Combined with the two antibacterial tests, it can be concluded that the PVDF/MWNTs-g-CDDAC hybrid membranes have good efficiency in suppressing the growth of E. coli and S. aureus.

4. Conclusions

In this work, N-halamine functionalized MWNTs, MWNTs grafted with

(3-chloro-2-hydroxypropyl)-(5,5-dimethylhydantoinyl-1-ylmethyl)-dimethylam-monium chloride (MWNTs-g-CDDAC) are synthesized and characterized. Then, the synthesized MWNTs-g-CDDAC are employed to fabricate one kind of novel PVDF/MWNTs-g-CDDAC hollow fiber ultrafiltraiton membranes with antibacterial and antifouling properties. The results show that with the addition of MWNTs-g-CDDAC in the dopes, the sponge-like structure is suppressed and the finger-like macrovoids grow wider for the membranes. The introduced MWNTs-g-CDDAC can evidently improve surface hydrophlicity, permeability and antifouling ability of the resulted membranes. The highest pure water permeability of 94.7 $L \cdot m^{-2} \cdot bar^{-1} \cdot h^{-1}$ is obtained with 0.50% MWNTs-g-CDDAC addition in the dope. The permeation flux recovery ratio (R_f) increases with the addition of MWNTs-g-CDDAC, and M-75 exhibits the highest R_f value of 90.6% after two ultrafiltration-cleaning cycles for BSA aqueous solution. The fabricated PVDF/MWNTs-g-CDDAC membranes have favourable antibacterial efficacy, and M-75 shows the utmost sterilization ratios of 92.7% and 95.2% against E. coli and S. aureus respectively.

Acknowledgements

The research is supported by Science and Technology Commission of Shanghai Municipality (13ZR1429900, 14520502900) and International Joint Laboratory on Resource Chemistry (IJLRC).

Nomenclature

J_w-pure water permeability ($L \cdot M^{-2} \cdot H^{-1} \cdot bar^{-1}$)

R-the rejection for solute (%).

Q-the volumetric flow rate ($L \cdot H^{-1}$).

ΔP-the transmembrane pressure (bar/Pa).

A-the effective membrane area (m^{-2}).

C_P-the concentrations of permeate (g/L).

C_F-the concentrations of feed solutions (g/L).

MWCO- molecular weight cut-off.

d_p -pore size of membranes.

ε -porosity(%)

N -the normality of the consumed $Na_2S_2O_3$ in the titration(eqv/L).

V-the volumeof the consumed $Na_2S_2O_3$ in the titration (L).

W-the weight of membrane sample in the titration(g).

E-the percentage of bacterial reduction(%).

n_0- the absorbance value of live bacterial cells in the flask contained the pristine PVDF membrane for shake flask method, or the colony number on the petri dish for spread plate method.

n_1- the absorbance value of live bacterial cells in the flask contained various PVDF/MWNTs-g-CDDAC membranes for the shake flask method, or the colony number on the petri dish for spread plate method.

R_f -flux recovery ratio (%)

References

1. J. Mansouri, S. Harrisson and V. Chen, *Journal of Materials Chemistry*, 2010, **20**, 4567-4586.
2. G.-d. Kang and Y.-m. Cao, *Journal of Membrane Science*, 2014, **463**, 145-165.
3. F. Liu, N. A. Hashim, Y. Liu, M. R. M. Abed and K. Li, *Journal of Membrane Science*, 2011, **375**, 1-27.
4. R. A. Damodar, S.-J. You and H.-H. Chou, *Journal of Hazardous Materials*, 2009, **172**, 1321-1328.
5. J. Dang, Y. Zhang, Z. Du, H. Zhang and J. Liu, *Water Science & Technology*, 2012, **66**, 799-803.
6. C. Liao, P. Yu, J. Zhao, L. Wang and Y. Luo, *Desalination*, 2011, **272**, 59-65.
7. H. Shi, F. Liu and L. Xue, *Journal of Membrane Science*, 2013, **437**, 205-215.
8. X. Li, R. Pang, J. Li, X. Sun, J. Shen, W. Han and L. Wang, *Desalination*, 2013, **324**, 48-56.
9. A. Rahimpour, M. Jahanshahi, B. Rajaeian and M. Rahimnejad, *Desalination*, 2011, **278**, 343-353.
10. I. Sawada, R. Fachrul, T. Ito, Y. Ohmukai, T. Maruyama and H. Matsuyama, *Journal of Membrane Science*, 2012, **387**, 1-6.
11. H. A. Shawky, S.-R. Chae, S. Lin and M. R. Wiesner, *Desalination*, 2011, **272**, 46-50.
12. V. Vatanpour, S. S. Madaeni, R. Moradian, S. Zinadini and B. Astinchap, *Journal of Membrane Science*, 2011, **375**, 284-294.
13. Y. Mansourpanah, S. S. Madaeni, A. Rahimpour, M. Adeli, M. Y. Hashemi and M. R. Moradian, *Desalination*, 2011, **277**, 171-177.
14. E. Celik, H. Park, H. Choi and H. Choi, *Water Research*, 2011, **45**, 274-282.
15. A. Rahimpour, M. Jahanshahi, S. Khalili, A. Mollahosseini, A. Zirepour and B. Rajaeian, *Desalination*, 2012, **286**, 99-107.
16. S. Majeed, D. Fierro, K. Buhr, J. Wind, B. Du, A. Boschetti-de-Fierro and V. Abetz, *Journal of Membrane Science*, 2012, **403–404**, 101-109.
17. S. S. Madaeni, S. Zinadini and V. Vatanpour, *Separation and Purification Technology*, 2013, **111**, 98-107.
18. M. J. Gallagher, H. Huang, K. J. Schwab, D. H. Fairbrother and B. Teychene, *Journal of Membrane Science*, 2013, **446**, 59-67.
19. V. Vatanpour, M. Esmaeili and M. H. D. A. Farahani, *Journal of Membrane Science*, 2014, **466**, 70-81.
20. X. Zhang, W.-Z. Lang, H.-P. Xu, X. Yan, Y.-J. Guo and L.-F. Chu, *Journal of Membrane Science*, 2014, **469**, 458-470.
21. L. Bai, H. Liang, J. Crittenden, F. Qu, A. Ding, J. Ma, X. Du, S. Guo and G. Li, *Journal of Membrane Science*, 2015, **492**, 400-411.
22. N. Ghaemi, S. S. Madaeni, P. Daraei, H. Rajabi, T. Shojaeimehr, F. Rahimpour and B. Shirvani, *Journal of Hazardous Materials*, 2015, **298**, 111-121.
23. L. Stobinski, B. Lesiak, L. Kövér, J. Tóth, S. Biniak, G. Trykowski and J. Judek, *Journal of Alloys and Compounds*, 2010, **501**, 77-84.
24. I. Sawada, R. Fachrul, T. Ito, Y. Ohmukai, T. Maruyama and H. Matsuyama, *Journal of Membrane Science*, 2012, **387–388**, 1-6.

25. Y. Chen, Y. Zhang, J. Liu, H. Zhang and K. Wang, *Chemical Engineering Journal*, 2012, **210**, 298-308.
26. Y. H. Kim, D. K. Lee, H. G. Cha, C. W. Kim and Y. S. Kang, *The Journal of Physical Chemistry C*, 2007, **111**, 3629-3635.
27. A. Dong, S. Lan, J. Huang, T. Wang, T. Zhao, W. Wang, L. Xiao, X. Zheng, F. Liu, G. Gao and Y. Chen, *Journal of Colloid and Interface Science*, 2011, **364**, 333-340.
28. Z.-Z. Kang, B. Zhang, Y.-C. Jiao, Y.-H. Xu, Q.-Z. He and J. Liang, *Cellulose*, 2012, **20**, 885-893.
29. K. Tan and S. K. Obendorf, *Journal of Membrane Science*, 2007, **289**, 199-209.
30. K. Tan and S. K. Obendorf, *Journal of Membrane Science*, 2007, **305**, 287-298.
31. X. Wei, Z. Wang, J. Chen, J. Wang and S. Wang, *Journal of Membrane Science*, 2010, **346**, 152-162.
32. R. H. Bradley, K. Cassity, R. Andrews, M. Meier, S. Osbeck, A. Andreu, C. Johnston and A. Crossley, *Applied Surface Science*, 2012, **258**, 4835-4843.
33. Z.-Z. Kang, B. Zhang, Y.-C. Jiao, Y.-H. Xu, Q.-Z. He and J. Liang, *Cellulose*, 2013, **20**, 885-893.
34. W.-Z. Lang, Q. Ji, J.-P. Shen, Y.-J. Guo and Z.-L. Xu, *Desalination*, 2012, **292**, 45-52.
35. W.-Z. Lang, Z.-L. Xu, H. Yang and W. Tong, *Journal of Membrane Science*, 2007, **288**, 123-131.
36. W. Zhao, Y. Su, C. Li, Q. Shi, X. Ning and Z. Jiang, *Journal of Membrane Science*, 2008, **318**, 405-412.
37. H.-P. Xu, Y.-H. Yu, W.-Z. Lang, X. Yan and Y.-J. Guo, *RSC Advances*, 2015.
38. X. Zhang, W.-Z. Lang, H.-P. Xu, X. Yan and Y.-J. Guo, *RSC Advances*, 2015, **5**, 21532-21543.
39. B. Zhang, Y. Jiao, Z. Kang, K. Ma, X. Ren and J. Liang, *Cellulose*, 1-11.
40. L. Cen, K. G. Neoh and E. T. Kang, *Langmuir*, 2003, **19**, 10295-10303.
41. D. Xu, X. Tan, C. Chen and X. Wang, *Journal of Hazardous Materials*, 2008, **154**, 407-416.
42. X. Cheng, K. Ma, R. Li, X. Ren and T. S. Huang, *Applied Surface Science*, 2014, **309**, 138-143.
43. I. Cerkez, H. B. Kocer, S. D. Worley, R. M. Broughton and T. S. Huang, *Reactive and Functional Polymers*, 2012, **72**, 673-679.
44. H. B. Kocer, I. Cerkez, S. D. Worley, R. M. Broughton and T. S. Huang, *ACS Applied Materials & Interfaces*, 2011, **3**, 2845-2850.
45. L. Duan, W. Huang and Y. Zhang, *RSC Advances*, 2015, **5**, 6666-6674.
46. Y. V. Larichev, B. L. Moroz and V. I. Bukhtiyarov, *Applied Surface Science*, 2011, **258**, 1541-1550.
47. F.-C. Chiu, *Materials Chemistry and Physics*, 2014, **143**, 681-692.
48. Y. Liu and S. Kumar, *ACS Applied Materials & Interfaces*, 2014, **6**, 6069-6087.
49. D. Wu, J. Wang, M. Zhang and W. Zhou, *Industrial & Engineering Chemistry Research*, 2012, **51**, 6705-6713.
50. F. Liu, Y.-Y. Xu, B.-K. Zhu, F. Zhang and L.-P. Zhu, *Journal of Membrane Science*, 2009, **345**, 331-339.
51. H.-P. Xu, W.-Z. Lang, X. Yan, X. Zhang and Y.-J. Guo, *Journal of Membrane Science*, 2014, **467**, 142-152.
52. H. Yu, X. Zhang, Y. Zhang, J. Liu and H. Zhang, *Desalination*, 2013, **326**, 69-76.

53. L. Yu, Y. Zhang, B. Zhang, J. Liu, H. Zhang and C. Song, *Journal of Membrane Science*, 2013, **447**, 452-462.

Figure catptions

Fig. 1 The schematic diagram of MWNTs-OH.

Fig. 2 The route of synthesis of MWNTs-g-CDDAC.

Fig. 3 The FTIR spectra of MWNTs, MWNTs-OH and MWNTs-g-CDDAC (a), the digital photos of MWNTs, MWNTs-OH and MWNTs-g-CDDAC dispersed in absolute NMP for 30 days (b).

Fig. 4 The overall spectra of purified MWNTs, MWNTs-OH and MWNTs-g-CDDAC.

Fig. 5 The single element spectra of MWNTs, MWNTs-OH and MWNTs-g-CDDAC.

Fig. 6 The TGA curves of MWNTs, MWNTs-OH, MWNTs-g-CDDAC.

Fig. 7 The viscosity versus shear rate of different dope solutions.

Fig. 8 The FESEM images of the cross-section of PVDF/MWNTs-g-CDDAC hollow fiber membranes.

Fig. 9 The FESEM images of the outer surfaces of PVDF/MWNTs-g-CDDAC hollow fiber membranes.

Fig. 10 The FESEM images of the inner surfaces of PVDF/MWNTs-g-CDDAC hollow fiber membranes.

Fig. 11 The dynamic contact angles of PVDF/MWNTs-g-CDDAC hollow fiber membranes.

Fig. 12 Solute PEG rejection curves (a), probability density function curves (b) and cumulative pore size distribution curves (c) of PVDF/MWNTs-g-CDDAC hollow fiber membranes.

Fig. 13 Time-dependent flux of PVDF/MWNTs-g-CDDAC hollow fiber membranes with ultrafiltration and cleaning cycles.

Fig. 14 The antibacterial efficiency against E. coli of PVDF/MWNTs-g-CDDAC flat membranes (spread plate method).

Table captions